A Coarse Grained Stochastic Model of Translation Coupled Latent-Time Variability

Rui Ling[1], Wanqi Zhao[2], Yike Zhu[3], Ruoqing Zhang[4]
[1] Duke Kunshan University, [2] Nanjing Medical University, [3] Zhejiang University, [4] Westlake University

Abstract

Latent time, the interval between viral entry and release, is a central kinetic phenotype of lytic viral infection. In this study, we developed a coarse grained stochastic model to test how translation stage regulation can shape latent time variability. The model represents viral protein expression as five effective protein modules rather than experimentally annotated viral genes. Translation events are governed by module specific initiation preferences and probabilistic stop/readthrough decisions at inter module junctions, with a baseline stop:readthrough probability ratio of 2:1. Protein accumulation and degradation are simulated using a Gillespie style continuous time stochastic process, and release is defined as a first passage event in which all protein modules cross their module specific thresholds.

Across 500 baseline stochastic simulations, all infected cell simulations reached release within the simulation window. The mean latent time was 15.345 model time units, with a standard deviation of 1.909 and a coefficient of variation of 12.44%. A deterministic expected flow counterfactual using the same baseline parameters produced a single latent time of 14.311, corresponding to 0.933 after normalization to the stochastic baseline mean. Parameter uncertainty analysis across 200 parameter sets identified readthrough probability and translation event rate as the strongest single parameter associations with normalized mean latent time. Six of 200 parameter sets failed to produce any release within the simulation window, motivating explicit treatment of no release cases as censored outcomes. These results support the use of translation centered stochastic modeling as a hypothesis generating framework for identifying translation parameters that may influence latent time heterogeneity, while avoiding claims that the present coarse grained model fully explains real viral latent time.

Introduction

The latent period of a lytic viral infection is typically described as the time between successful entry into a host cell and release of newly produced viral particles. In bacteriophage biology, latent time and burst related phenotypes are often inferred from one step growth experiments, but population level curves can obscure substantial cell to cell heterogeneity. For compact positive strand RNA viruses and RNA bacteriophages, translation is not merely a passive step between

entry and replication; it can regulate the relative production of viral proteins through initiation accessibility, RNA structure, translational coupling, termination, and readthrough mechanisms.

The goal of this project was not to reconstruct the full intracellular life cycle of a specific virus. Instead, we asked a narrower modeling question: if only translation stage factors are varied, can a minimal stochastic first passage model generate interpretable changes in latent time timing and variability? This formulation is useful for a virtual modeling project because it isolates a mechanistic layer that is mathematically tractable while still biologically motivated.

To avoid overclaiming biological specificity, this manuscript refers to five effective viral protein modules rather than true viral genes. The modules represent coarse grained protein production requirements that must be met before release. This abstraction allows the model to incorporate translation initiation preference and stop/readthrough probabilities without pretending to map directly onto a real annotated genome.

Model Scope and Biological Interpretation

The model is a coarse grained stochastic first passage model of translation coupled latent time variability. It does not include viral genome replication, host cell resource limitation, immune response, capsid assembly kinetics, membrane lysis proteins, or experimentally measured gene specific rates. Therefore, the output should be interpreted as simulation based hypothesis generation rather than direct measurement of a real bacteriophage latent period.

Within this scope, the five modules can be understood as effective protein production requirements. A higher threshold means that more of that module must accumulate before release is possible. A higher initiation preference means translation events are more likely to begin at that module. Readthrough allows one translation event to produce downstream modules after passing an inter module junction, stopping terminates translation at the junction.

Mathematical Model

State Variables and Release Definition

Let $P_i(t)$ denote the abundance of protein module i at model time t, where $i = 1, \ldots, 5$. The system state is the vector $P(t) = [P_1(t), P_2(t), P_3(t), P_4(t), P_5(t)]$. Each module has a release threshold θ_i. Release is defined as a first-passage event:

$$T = \inf \{ t \geq 0 : P_i(t) \geq \theta_i, \forall\, i = 1, \ldots, 5 \}.$$

This definition means latent time is the first time at which all required modules have crossed their thresholds simultaneously. The module with the latest threshold crossing time is defined as the bottleneck module.

Translation Initiation Preference

Each translation event begins at one effective module. The start module S is sampled from a categorical distribution:

$$\Pr(S = i) = \alpha_i, \text{ where } \alpha_i \geq 0 \text{ and } \sum_i \alpha_i = 1.$$

In the baseline model, $\alpha = [0.45, 0.25, 0.15, 0.10, 0.05]$. This vector does not claim that a real viral ribosome randomly chooses among five annotated genes. Instead, it represents coarse grained translation initiation preference among effective protein production modules.

Stop and Readthrough Decisions

After translation begins at module S, the event produces module S. At each downstream intermodule junction, translation either stops or reads through to the next module. The baseline stop:readthrough probability ratio is 2:1, giving $p_{\text{stop}} = 2/3$ and $p_{\text{readthrough}} = 1/3$. If translation reads through from module j to $j + 1$, module $j + 1$ is also produced by the same translation event. The process continues until a stop event occurs or the final module is reached.

This representation makes readthrough mathematically equivalent to a mechanism that can couple production of downstream modules to an upstream translation event. Therefore, increases in readthrough probability should be interpreted carefully: they may shorten latent time partly because each translation event produces more total downstream protein output, not necessarily because real viruses use readthrough as a precise latent time control knob.

Gillespie Style Stochastic Kinetics

The model uses a continuous time stochastic simulation structure inspired by the Gillespie stochastic simulation algorithm. At each step, translation occurs with propensity $k_{\text{translation}}$, while degradation of module i occurs with propensity $k_{\text{degradation}} P_i$. The total event rate is:

$$a_0(P) = k_{\text{translation}} + \sum_i k_{\text{degradation}} P_i.$$

The waiting time to the next event is sampled from an exponential distribution with mean $1/a_0(P)$. The event identity is then sampled in proportion to its propensity. Translation events increase one or more modules according to the initiation and readthrough rules. Degradation events reduce one selected protein module by one molecule, bounded below by zero.

Deterministic Expected Flow Counterfactual

To avoid the trivial conclusion that stochastic input produces stochastic output, The final model includes a deterministic expected flow counterfactual. In this control, the expected output of one translation event is computed analytically. The expected output for module j is:

$$E[Y_j] = \sum_{i \leq j} \alpha_i \, p_{\text{readthrough}}^{\,j-i}.$$

The deterministic protein dynamics are then approximated by:

$$dP_j/dt = k_{translation}\, E[Y_j] - k_{degradation}\, P_j.$$

This counterfactual uses the same baseline parameters as the stochastic model but removes event level randomness in initiation, readthrough, waiting times, and degradation. Comparing stochastic and deterministic latent time behavior therefore directly addresses how much variability is contributed by translation stage stochasticity under the same parameter regime.

No Release and Censoring Treatment

If a simulation does not reach release before T_{max}, the latent time is recorded as missing for success only summaries. The final model additionally computes a censored latent time by assigning unreleased simulations the value T_{max}. This avoids hiding the fact that some parameter regimes are slow enough to fail within the observation window. The manuscript therefore reports both success only latent time statistics and release success rate.

Parameterization and Reproducibility

Parameter	Symbol	Baseline value	Interpretation
Number of modules	n	5	Five effective protein modules
Initiation preference	alpha	[0.45, 0.25, 0.15, 0.10, 0.05]	Relative initiation preference among modules
Readthrough probability	p_readthrough	1/3	Probability of crossing an intermodule junction
Stop probability	p_stop	2/3	Probability of terminating at a junction
Translation event rate	k_translation	20	Translation events per model time unit
Protein degradation rate	k_degradation	0.01	First order protein loss
Protein thresholds	theta	[120, 80, 60, 40, 30]	Module specific release requirements
Maximum simulation time	T_max	200	Censoring time for no release simulations
Baseline simulations	N	500	Number of stochastic baseline cells
Random seed	seed	42	Reproducibility setting

Table 1. Baseline model parameters used in the final model.

Parameter	Sampling distribution	Value or range
Readthrough probability	Uniform(0.10, 0.60)	0.10 to 0.60
Translation event rate	Uniform(10, 40)	10 to 40
Protein degradation rate	Uniform(0.001, 0.03)	0.001 to 0.03
Initiation preference alpha	Dirichlet([4.5, 2.5, 1.5, 1.0, 0.5])	Sums to 1
Protein thresholds	Baseline threshold x Uniform(0.75, 1.25)	75% to 125% of baseline
Parameter sets	Fixed	200
Simulations per parameter set	Fixed	30

Table 2. Parameter uncertainty sampling design.

Results

Baseline Latent Time Variability

All 500 baseline stochastic simulations reached release within the simulation window. The mean latent time was 15.345 model time units, the median latent time was 15.096, and the standard deviation was 1.909. The resulting coefficient of variation was 12.44%, indicating moderate stochastic dispersion around the baseline mean.

The deterministic expected flow control reached release at 14.311 model time units, or 0.933 after normalization to the stochastic baseline mean. Because this deterministic control has no event level randomness under fixed parameters, it provides a counterfactual reference for interpreting the stochastic latent time distribution.

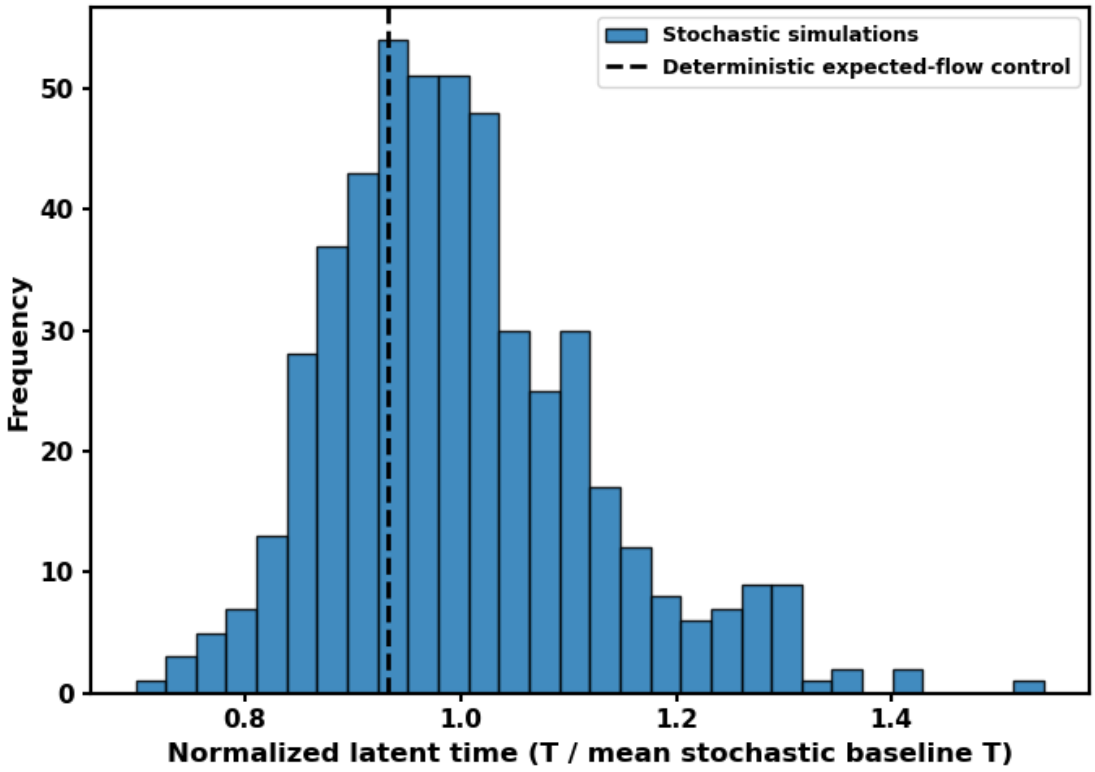

Figure 1. Normalized baseline latent time distribution compared with the deterministic expected flow control.

Example Single Cell Trajectory

One representative stochastic trajectory reached release at latent time 16.017. Protein module 1 was the bottleneck module in this example. The normalized trajectory shows that modules crossed the release threshold at different times, illustrating how first passage timing depends on the slowest required module rather than on total protein production alone.

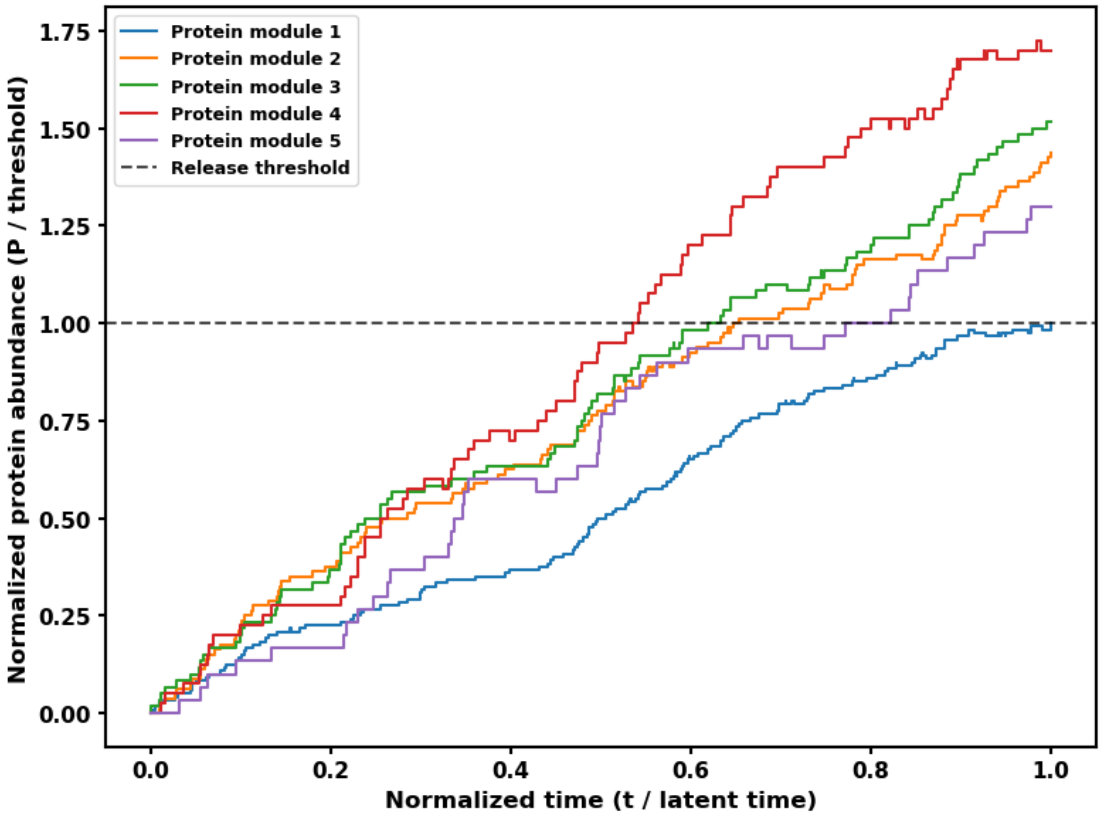

Figure 2. Normalized protein trajectory for one stochastic infected cell simulation.

Bottleneck Module Identity

Under baseline parameters, Protein module 1 was the bottleneck in 295 of 500 simulations (59.0%), while Protein module 5 was the bottleneck in 187 simulations (37.4%). The other modules were rarely the final threshold crossing module. This pattern should not be interpreted as a discovery about true viral genes; rather, it reflects the interaction between initiation preference, readthrough structure, and the chosen module thresholds.

Module	Count	Percentage
Protein module 1	295	59.0%
Protein module 2	1	0.2%
Protein module 3	10	2.0%
Protein module 4	7	1.4%
Protein module 5	187	37.4%

Table 3. Baseline bottleneck module distribution.

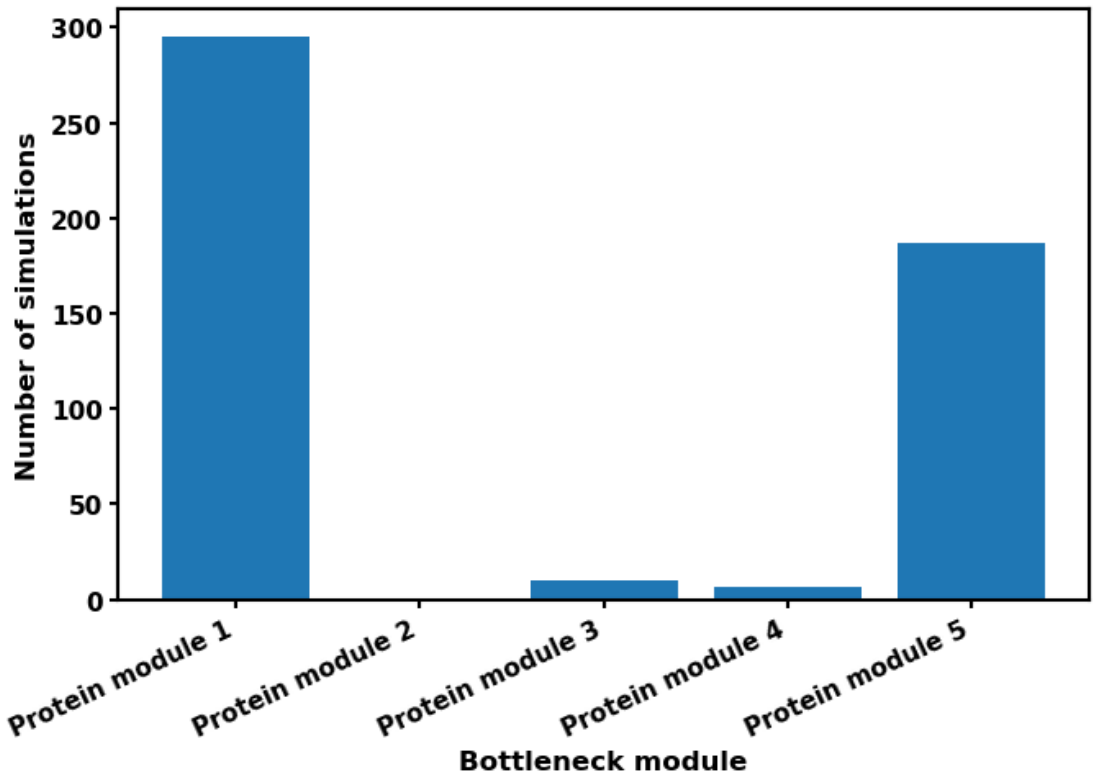

Figure 3. Baseline bottleneck module counts.

Threshold Crossing Order

Mean normalized threshold crossing times showed that Protein modules 2, 3, and 4 generally crossed thresholds earlier than modules 1 and 5. Protein module 1 had the latest mean normalized crossing time (0.935), followed by Protein module 5 (0.897). This explains why bottleneck identity was concentrated in these two modules.

Module	Mean normalized crossing time
Protein module 1	0.935
Protein module 2	0.689
Protein module 3	0.729
Protein module 4	0.705
Protein module 5	0.897

Table 4. Mean normalized threshold crossing times.

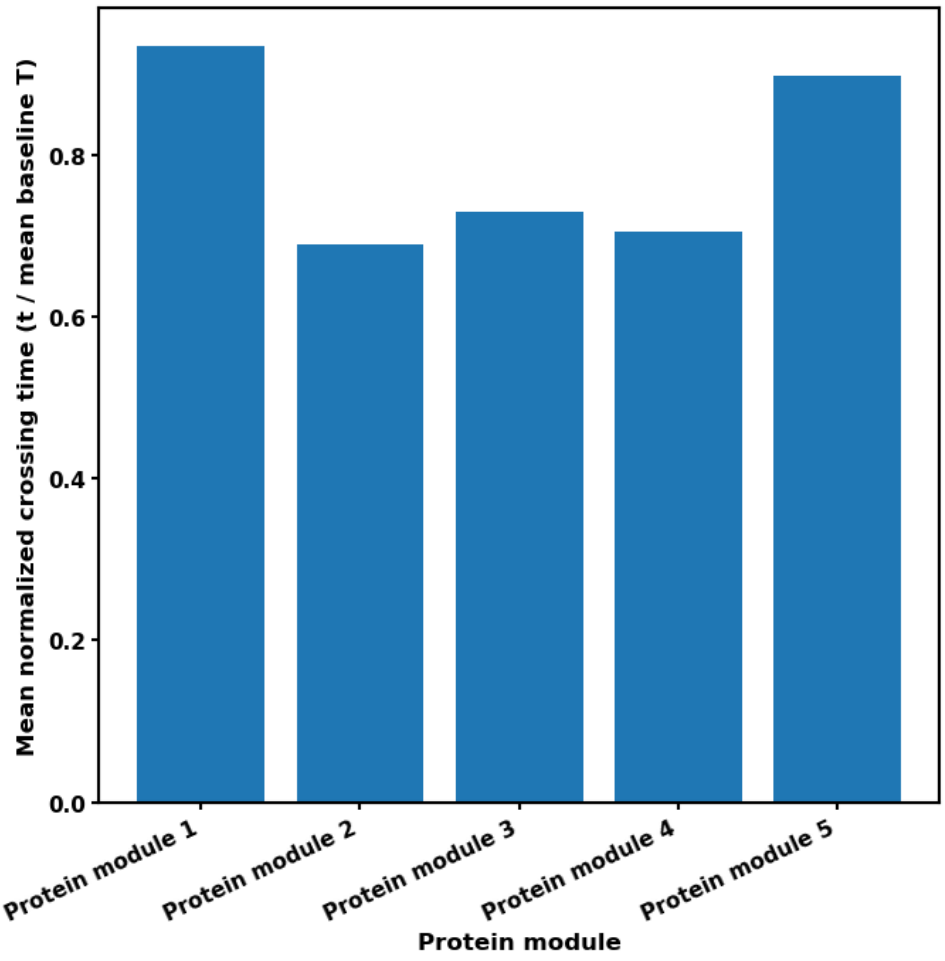

Figure 4. Mean normalized crossing time by protein module.

Non-Bottleneck Excess at Release

Because release is defined as the first time all modules exceed their thresholds, the minimum ratio P_i/θ_i is expected to be close to 1 at release. The final model therefore focuses on non-bottleneck excess: the average surplus above threshold among modules that were not the bottleneck. The baseline mean non-bottleneck excess was 0.327, suggesting that when the final module reaches threshold, other modules have often accumulated moderate surplus.

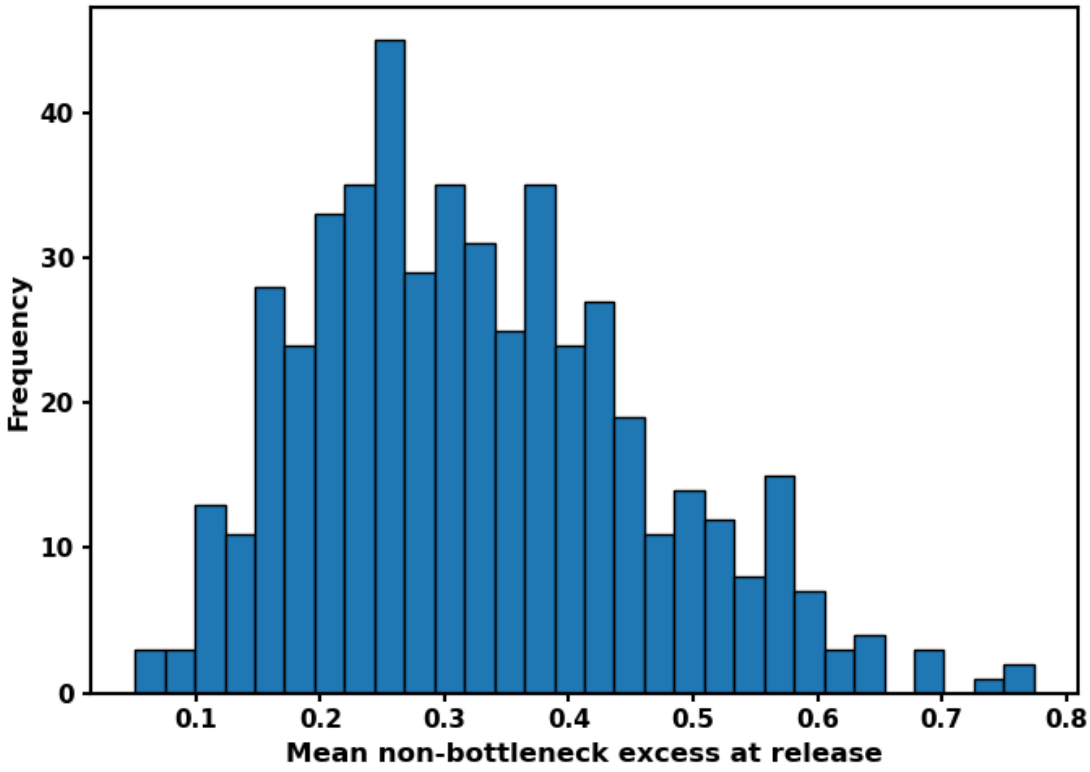

Figure 5. Distribution of mean non-bottleneck excess at release.

Parameter Uncertainty and No Release Cases

Across 200 sampled parameter sets, 194 had at least one successful release among 30 stochastic simulations, while 6 parameter sets had no release within T_{max}. The mean release success rate across all parameter sets was 0.9315. For success only parameter sets, normalized mean latent time had a mean of 2.216, median of 1.334, and maximum of 12.023. When no release simulations were treated as censored at T_{max}, normalized mean latent time increased, highlighting the importance of reporting no release behavior rather than excluding it silently.

Metric	Value
Total parameter sets	200
Parameter sets with at least one release	194
Parameter sets with no release	6
Mean release success rate	0.9315
Mean normalized latent time, success-only	2.216
Median normalized latent time, success-only	1.334
Maximum normalized latent time, success-only	12.023

Table 5. Robustness and no release summary.

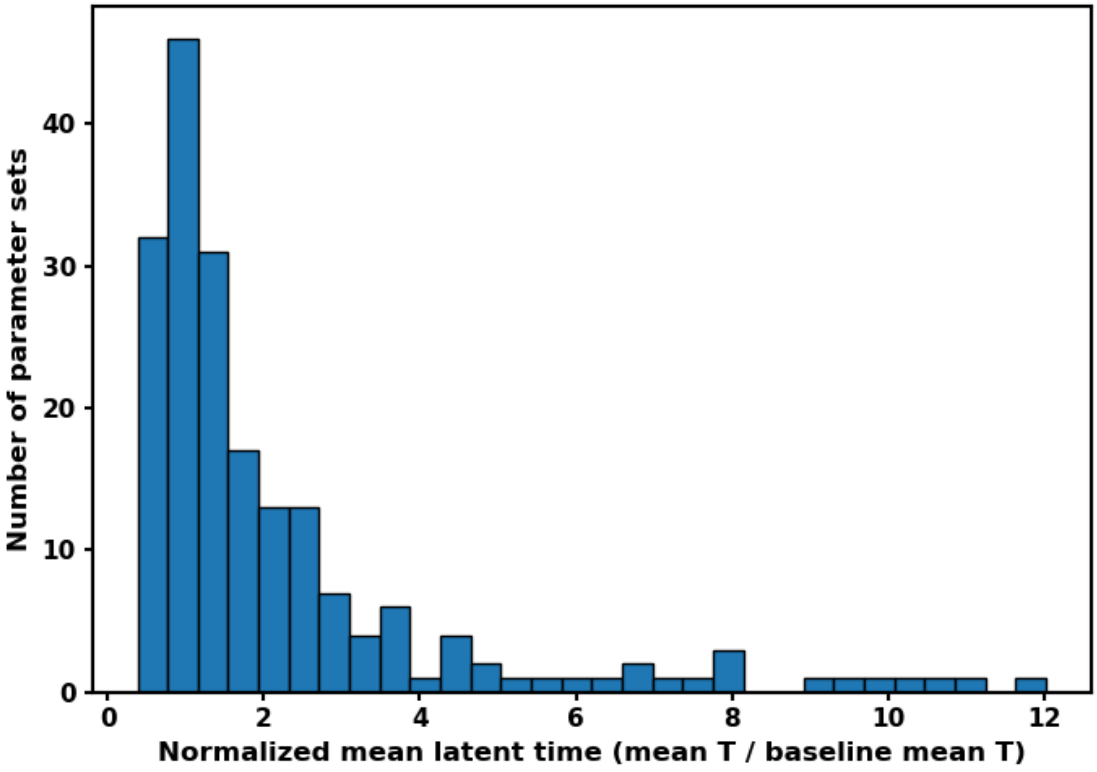

Figure 6. Distribution of normalized mean latent time across parameter sets.

Parameter Associations with Latent Time

Readthrough probability showed the strongest single parameter association with normalized mean latent time (Pearson $r = –0.419$, $p = 1.15 \times 10^{–9}$), followed by translation event rate ($r = –0.348$, $p = 6.88 \times 10^{–7}$). Both associations remained significant after FDR correction. The negative direction indicates that higher readthrough probability and higher translation event rate were associated with shorter simulated latent time. These are moderate simulation-based associations, not experimental causal estimates.

Parameter	n	Pearson r	p value	95% CI	FDR p
p_readthrough	194	-0.419	1.15e-09	[-0.529, -0.296]	1.49e-08
k_translation	194	-0.348	6.88e-07	[-0.466, -0.217]	4.47e-06
threshold_2	194	0.094	0.190	[-0.047, 0.232]	0.749
alpha_5	194	-0.091	0.205	[-0.229, 0.050]	0.749
threshold_4	194	0.079	0.275	[-0.063, 0.217]	0.749

Table 6. Top parameter associations with normalized mean latent time.

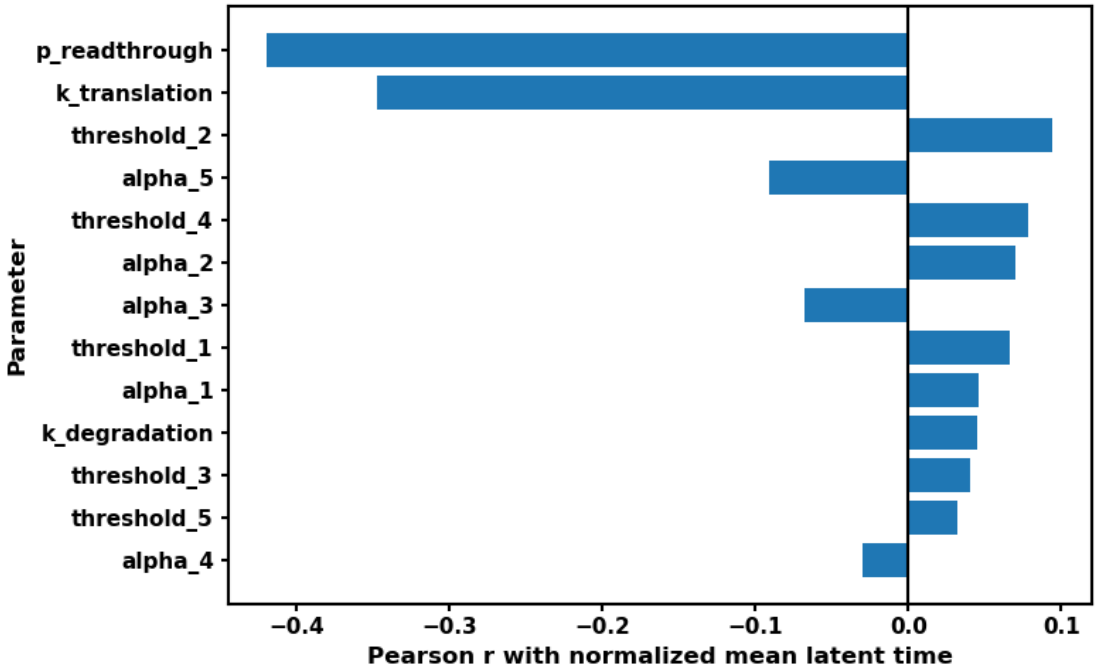

Figure 7. Pearson correlations between sampled parameters and normalized mean latent time.

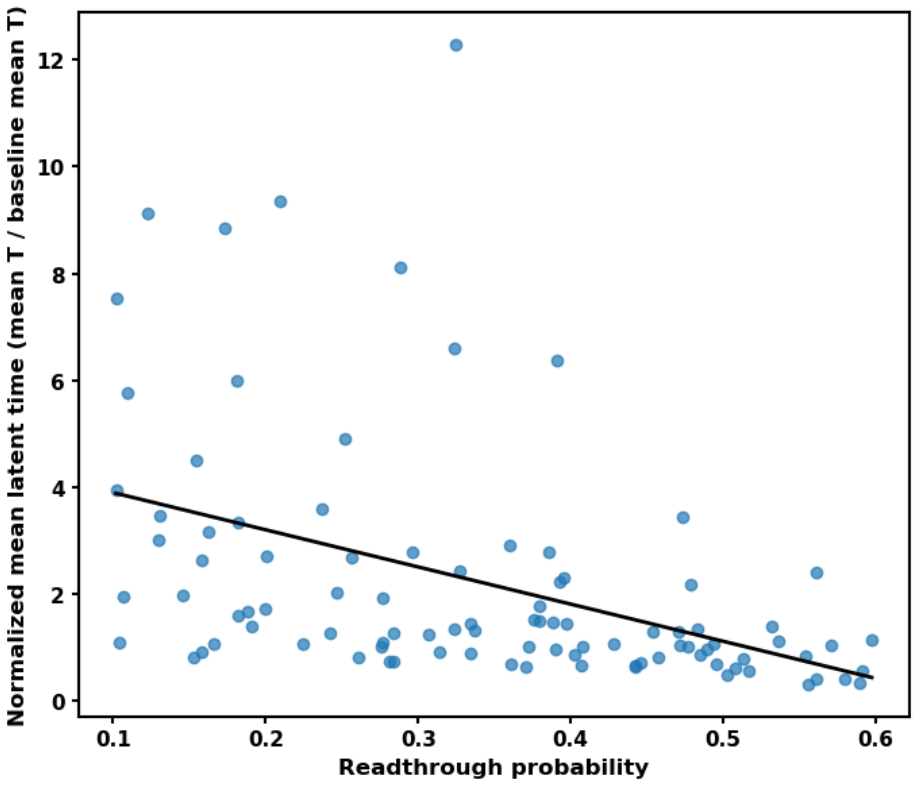

Figure 8. Readthrough probability versus normalized mean latent time with regression line and 95% confidence interval.

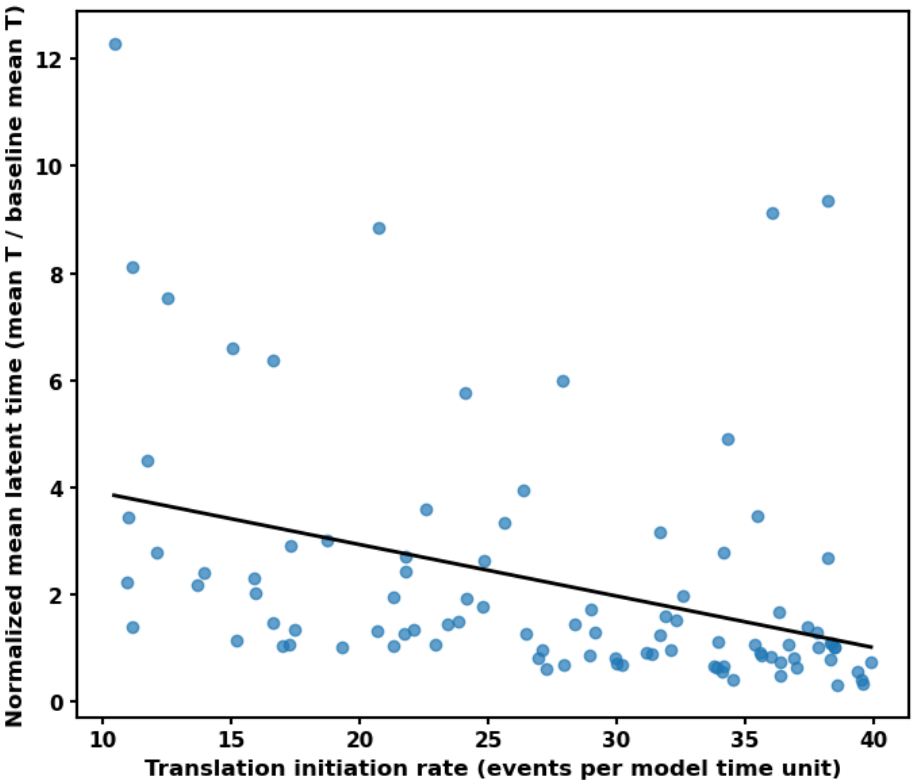

Figure 9. Translation event rate versus normalized mean latent time with regression line and 95% confidence interval.

Release Success Rate

The release success-rate plots evaluate whether sampled parameter sets reached the release threshold within the observation window. Each point represents one sampled parameter set, and the y-axis shows the fraction of 30 stochastic simulations that successfully released before T_{max}. Most points are concentrated near a success rate of 1.0, indicating that most parameter regimes produced release reliably. A small number of parameter sets showed reduced or zero success, suggesting that some combinations of low productive translation or unfavorable thresholds can delay protein accumulation beyond the simulation window.

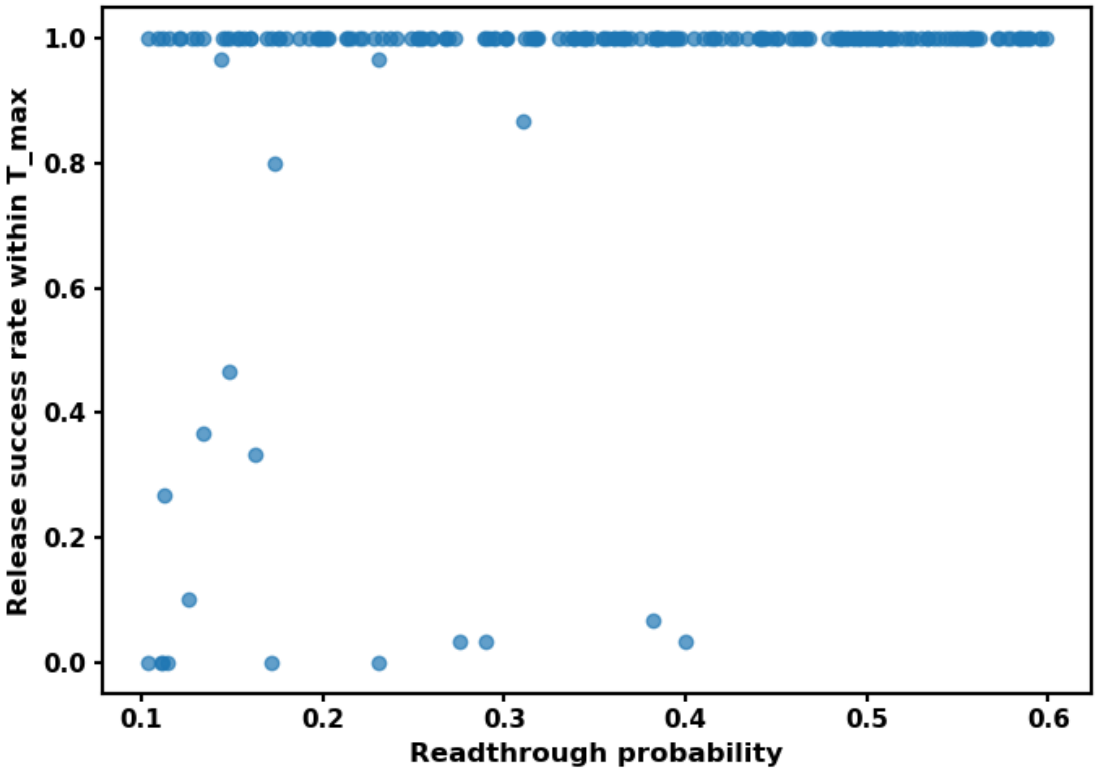

Figure 10A. Release success rate across sampled readthrough probabilities.

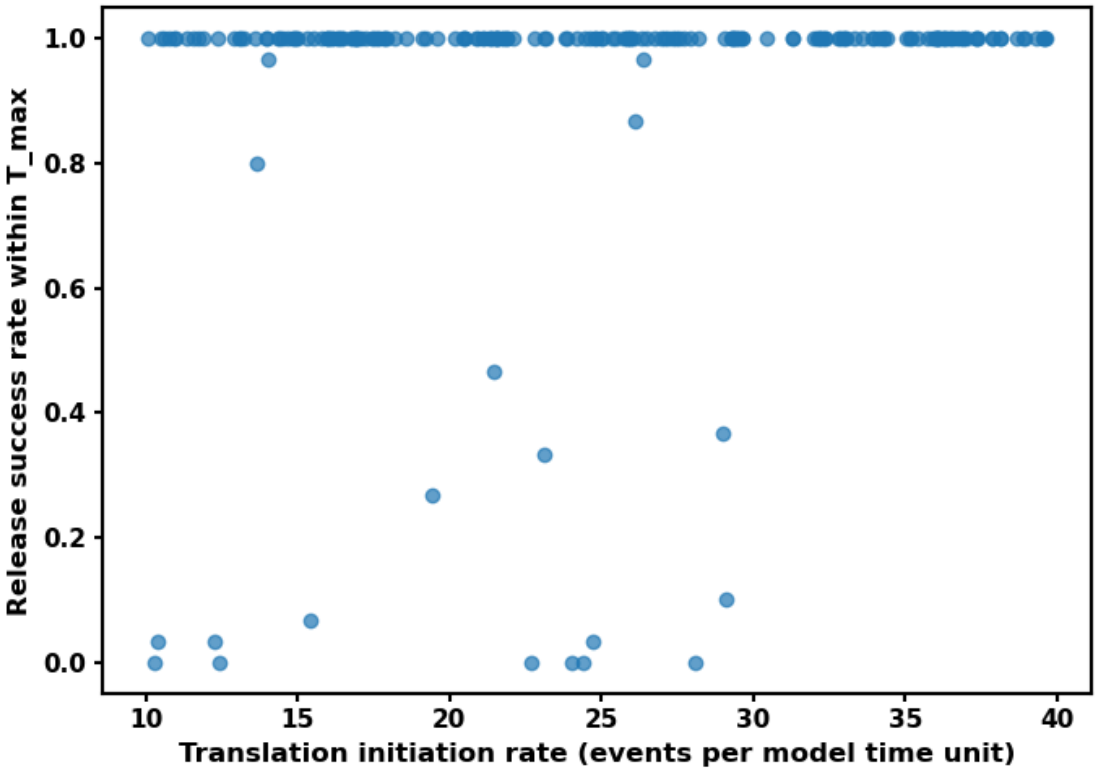

Figure 10B. Release success rate across sampled readthrough probabilities and translation event rates.

Bottleneck Robustness and Threshold Sensitivity

Across valid robustness parameter sets, Protein module 1 remained the most common bottleneck in 91 parameter sets (46.9%), followed by Protein module 5 in 56 sets (28.9%). However, the identity of the bottleneck was parameter regime dependent. A dedicated θ_1 sensitivity analysis showed that as the Module 1 threshold increased from 0.6 to 1.4 times its baseline value, the fraction of simulations in which Module 1 was the bottleneck increased from 0.00 to 0.97. This supports the interpretation that the baseline bottleneck pattern is driven by parameter structure, especially the threshold assigned to Module 1, rather than by a universal biological rule.

Module	Parameter-set count	Percentage
Protein module 1	91	46.9%
Protein module 2	17	8.8%
Protein module 3	12	6.2%
Protein module 4	18	9.3%
Protein module 5	56	28.9%

Table 7. Most common bottleneck module across parameter sets.

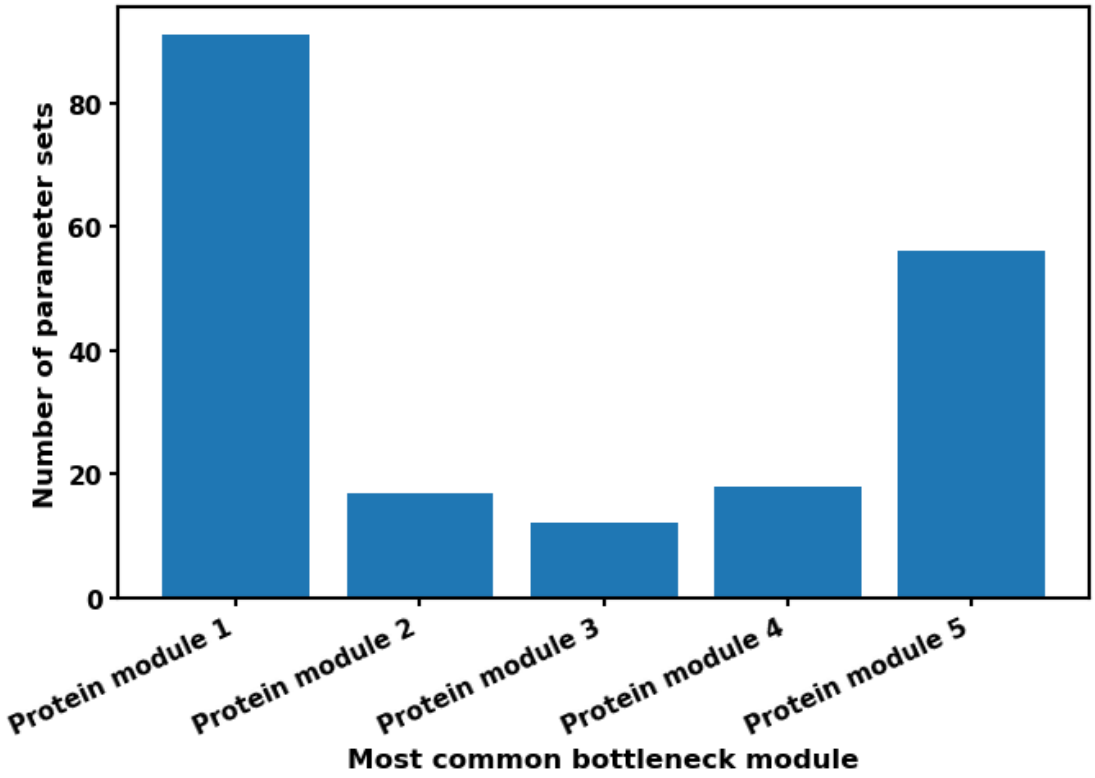

Figure 11. Bottleneck robustness across parameter sets.

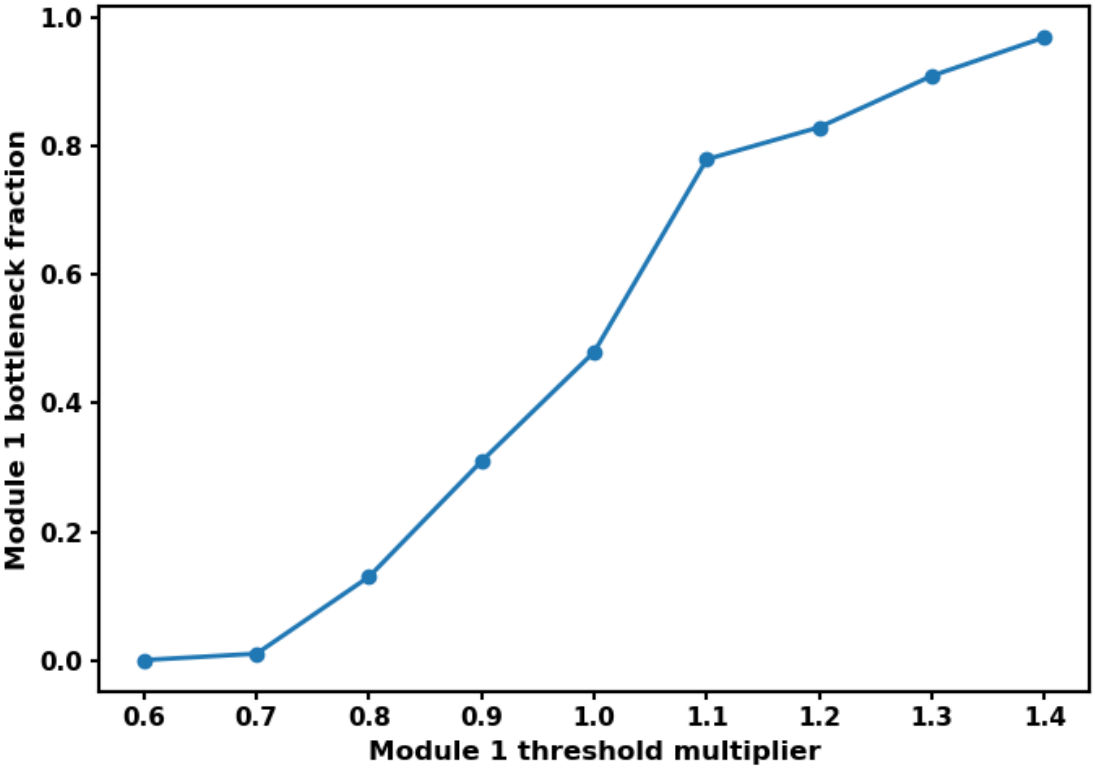

Figure 12. θ_1 sensitivity analysis.

Discussion

This study demonstrates how translation stage mechanisms can be represented in a compact stochastic first passage model of latent time variability. The main methodological contribution is the integration of initiation preference, probabilistic stop/readthrough, protein degradation, threshold based release, deterministic counterfactual control, and censored no release analysis in a single reproducible simulation framework.

The baseline stochastic model produced a latent time CV of 12.44%, while the deterministic expected flow counterfactual produced a single release time under fixed parameters. This comparison is important because it prevents the central claim from collapsing into the trivial statement that stochastic models produce distributions. Instead, the result shows that event level stochasticity in translation is sufficient to generate measurable first passage variability under the chosen parameter regime.

The strongest parameter association was between readthrough probability and normalized mean latent time. This result is mechanistically plausible within the model because higher readthrough increases downstream module production per translation event. However, this interpretation should remain model specific. It does not prove that biological readthrough alone regulates real viral latent periods, especially because real RNA viruses may involve overlapping genes, RNA secondary structure, subgenomic RNAs, frameshifting, genome replication, assembly, and host cell constraints.

The bottleneck analysis further shows why model transparency matters. Module 1 had the highest initiation preference but also the highest threshold. Therefore, its frequent appearance as the bottleneck is not paradoxical; it reflects a balance between production preference and release requirement. The threshold sensitivity analysis makes this parameter dependence explicit.

Limitations

This study has several important limitations. First, the model is intentionally coarse-grained and does not represent experimentally annotated viral genes. The five protein modules should be interpreted as effective protein-production requirements rather than true gene identities. Second, the parameters used in the simulations, including initiation preference, readthrough probability, translation rate, degradation rate, and release thresholds, were selected for exploratory modeling rather than fitted to experimental measurements. Third, release was modeled as a first-passage threshold-crossing event and did not explicitly include genome replication, virion assembly, genome packaging, host-cell resource limitation, spatial organization, or lysis-protein kinetics. Fourth, inter-module junctions were represented phenomenologically by stop/readthrough

probabilities rather than by explicit RNA sequence or secondary-structure modeling. Fifth, parameter associations reflect simulated correlations within the selected sampling ranges and should not be interpreted as experimental causal effects. Finally, the model has not yet been experimentally validated and should be used as a hypothesis-generating framework rather than as a complete explanation of real viral latent time.

Future Directions

The most direct next step is to map the effective modules onto a specific model virus, such as a well characterized positive strand RNA bacteriophage, and assign initiation probabilities, readthrough or translational coupling parameters, and thresholds from literature or experimental measurements. A second extension would incorporate genome replication and assembly explicitly, allowing the model to distinguish translation limited, replication limited, and assembly limited regimes. A third direction is to replace simple pairwise correlations with multivariable regression or global sensitivity analysis, which would better capture parameter interactions.

Conclusion

This study provides a reproducible coarse grained mathematical model for studying how translation stage parameters can shape simulated latent time variability. By adding a deterministic counterfactual, statistical correlation testing, no release analysis, and threshold sensitivity analysis, the model addresses key interpretability concerns and supports a more cautious conclusion: translation stage stochasticity can contribute to latent time variability in a simplified first passage framework, but the model should be used to generate hypotheses rather than to claim complete mechanistic explanation of real viral latent time.

References

COVID. (n.d.). In *www.mdpi.com*. Retrieved August 3, 2026, from https://www.mdpi.com/journal/covid

Alexandersen, S., Chamings, A., & Bhatta, T. R. (2020). SARS-CoV-2 genomic and subgenomic RNAs in diagnostic samples are not an indicator of active replication. *Nature Communications*, *11*(1), 6059. https://doi.org/10.1038/s41467-020-19883-7

Sun, L., Li, P., Ju, X., Ren, R., Huang, W., Ren, L., Wu, Y., Xiong, T., Xu, K., Zhou, X., Gong, M., Miska, E. A., Ding, Q., Wang, J., & Qiangfeng Cliff Zhang. (2021). *In vivo structural characterization of the SARS-CoV-2 RNA genome identifies host proteins vulnerable to repurposed drugs*. *184*(7), 1865–1883.e20. https://doi.org/10.1016/j.cell.2021.02.008

Subong, B. J. J., & Forteza, I. L. (2025). SARS-CoV-2 Replication Revisited: Molecular Insights and Current and Emerging Antiviral Strategies. *Covid*, *5*(6), 85. https://doi.org/10.3390/covid5060085

Mohammadi, E., Shafiee, F., Shahzamani, K., Ranjbar, M. M., Alibakhshi, A., Ahangarzadeh, S., Beikmohammadi, L., Shariati, L., Hooshmandi, S., Ataei, B., & Javanmard, S. H. (2021). Novel and emerging mutations of SARS-CoV-2: Biomedical implications. *Biomedicine & Pharmacotherapy = Biomedecine & Pharmacotherapie*, *139*, 111599. https://doi.org/10.1016/j.biopha.2021.111599

Zhang, Y., Zhang, X., Zheng, H., & Liu, L. (2022). Subgenomic RNAs and Their Encoded Proteins Contribute to the Rapid Duplication of SARS-CoV-2 and COVID-19 Progression. *Biomolecules*, *12*(11), 1680. https://doi.org/10.3390/biom12111680

Hayn, M., Hirschenberger, M., Koepke, L., Nchioua, R., Straub, J. H., Klute, S., Hunszinger, V., Zech, F., Bozzo, C. P., Aftab, W., Christensen, M. H., Conzelmann, C., Müller, J. A., Badarinarayan, S. S., Stürzel, C. M., Forne, I., Stenger, S., Conzelmann, K.-K., Münch, J., … Johannes Sparrer, K. M. (2021). Systematic Functional Analysis of SARS-CoV-2 Proteins Uncovers Viral Innate Immune Antagonists and Remaining Vulnerabilities. *Cell Reports*, 109126. https://doi.org/10.1016/j.celrep.2021.109126

Hartenian, E., Nandakumar, D., Lari, A., Ly, M., Tucker, J. M., & Glaunsinger, B. A. (2020). The molecular virology of Coronaviruses. *Journal of Biological Chemistry*, *295*(37), jbc.REV120.013930. https://doi.org/10.1074/jbc.rev120.013930

Chang, K.-C., & Wen, J.- Der. (2021). Programmed −1 ribosomal frameshifting from the perspective of the conformational dynamics of mRNA and ribosomes. *Computational*

and Structural Biotechnology Journal, *19*, 3580–3588. https://doi.org/10.1016/j.csbj.2021.06.015

Malone, B., Urakova, N., Snijder, E. J., & Campbell, E. A. (2021). Structures and functions of coronavirus replication–transcription complexes and their relevance for SARS-CoV-2 drug design. *Nature Reviews Molecular Cell Biology*, *23*(23). https://doi.org/10.1038/s41580-021-00432-z

Zimmermann, L., Zhao, X., Makroczyova, J., Moritz Wachsmuth-Melm, Prasad, V., Hensel, Z., Ralf Bartenschlager, & Petr Chlanda. (2023). SARS-CoV-2 nsp3 and nsp4 are minimal constituents of a pore spanning replication organelle. *Nature Communications*, *14*(1). https://doi.org/10.1038/s41467-023-43666-5

Huang, Y., Wang, T., Zhong, L., Zhang, W., Zhang, Y., Yu, X., Yuan, S., & Ni, T. (2024). Molecular architecture of coronavirus double-membrane vesicle pore complex. *Nature*. https://doi.org/10.1038/s41586-024-07817-y

Shestakova, E. D., Tumbinsky, R. S., Andreev, D. E., Rozov, F. N., Shatsky, I. N., & Terenin, I. M. (2023). The Roles of eIF4G2 in Leaky Scanning and Reinitiation on the Human Dual-Coding POLG mRNA. *International Journal of Molecular Sciences*, *24*(24), 17149. https://doi.org/10.3390/ijms242417149

Lama-Diaz, T., & Blanco, M. G. (2024). Alternative translation initiation by ribosomal leaky scanning produces multiple isoforms of the Pif1 helicase. *Nucleic Acids Research*, *52*(12), 6928–6944. https://doi.org/10.1093/nar/gkae400

Leaky scanning ~ ViralZone. (n.d.). In *viralzone.expasy.org*. Retrieved August 3, 2026, from https://viralzone.expasy.org/1976

Sun, Y., Abriola, L., Niederer, R. O., Pedersen, S. F., Alfajaro, M. M., Silva Monteiro, V., Wilen, C. B., Ho, Y.-C., Gilbert, W. V., Surovtseva, Y. V., Lindenbach, B. D., & Guo, J. U. (2021). Restriction of SARS-CoV-2 replication by targeting programmed −1 ribosomal frameshifting. *Proceedings of the National Academy of Sciences*, *118*(26). https://doi.org/10.1073/pnas.2023051118

Barndt, R. J., Liu, Q., Tang, Y., Haugh, M. P., Cui, J., Chan, S. Y., & Wu, H. (2022). Metabolic Maturation Exaggerates Abnormal Calcium Handling in a Lamp2 Knockout Human Pluripotent Stem Cell-Derived Cardiomyocyte Model of Danon Disease. *Biomolecules*, *13*(1), 69. https://doi.org/10.3390/biom13010069

Verma, R., Saha, S., Kumar, S., Mani, S., Maiti, T. K., & Surjit, M. (2021). RNA-Protein Interaction Analysis of SARS-CoV-2 5′ and 3′ Untranslated Regions Reveals a Role of Lysosome-Associated Membrane Protein-2a during Viral Infection. *mSystems*, *6*(4). https://doi.org/10.1128/msystems.00643-21

Yang, S. L., DeFalco, L., Wang, S., Wong, Y. H., Han, J., Mok, C. K., Tan, K. Y., Lim, S. Y., Zhao, Z., Zhang, Y., Lim, J. J. A., Xiang, J. S., Sobota, R., Wang, L.-F., Chu, J. J. H., Merits, A., Huber, R. G., & Wan, Y. (2025). A conserved long-range RNA interaction in SARS-CoV-2 recruits ADAR1 to enhance virus proliferation. *Nature Communications*, *16*(1). https://doi.org/10.1038/s41467-025-63297-2

Schubert, K., Karousis, E. D., Jomaa, A., Scaiola, A., Echeverria, B., Gurzeler, L.-A., Leibundgut, M., Thiel, V., Mühlemann, O., & Ban, N. (2020). SARS-CoV-2 Nsp1 binds the ribosomal mRNA channel to inhibit translation. *Nature Structural & Molecular Biology*, *27*(10), 959–966. https://doi.org/10.1038/s41594-020-0511-8

Zou, L., Moch, C., Graille, M., & Chapat, C. (2022). The SARS-CoV-2 protein NSP2 impairs the silencing capacity of the human 4EHP-GIGYF2 complex. *iScience*, *25*(7), 104646. https://doi.org/10.1016/j.isci.2022.104646

Khan, D., Terenzi, F., Liu, G., Ghosh, P., Ye, F., Nguyen, K., China, A., Iyappan Ramachandiran, Chakraborty, S., Stefan, J. A., Khan, K., Vasu, K. I., Dong, F., Willard, B., Karn, J., Gack, M. U., & Fox, P. L. (2023). A viral pan-end RNA element and host complex define a SARS-CoV-2 regulon. *Nature Communications*, *14*(1). https://doi.org/10.1038/s41467-023-39091-3

Ciupe, S. M., & Conway, J. M. (2024). Incorporating Intracellular Processes in Virus Dynamics Models. *Microorganisms*, *12*(5), 900. https://doi.org/10.3390/microorganisms12050900

Heldt, F. S., Frensing, T., & Reichl, U. (2012). Modeling the Intracellular Dynamics of Influenza Virus Replication To Understand the Control of Viral RNA Synthesis. *Journal of Virology*, *86*(15), 7806–7817. https://doi.org/10.1128/jvi.00080-12

Zitzmann, C., Schmid, B., Ruggieri, A., Perelson, A. S., Binder, M., Bartenschlager, R., & Kaderali, L. (2020). A Coupled Mathematical Model of the Intracellular Replication of Dengue Virus and the Host Cell Immune Response to Infection. *Frontiers in Microbiology*, *11*. https://doi.org/10.3389/fmicb.2020.00725

Dmitry Grebennikov, Ekaterina Kholodareva, Igor Sazonov, Karsonova, A., Meyerhans, A., & Gennady Bocharov. (2021). Intracellular Life Cycle Kinetics of SARS-CoV-2 Predicted

Using Mathematical Modelling. *Viruses*, *13*(9), 1735–1735. https://doi.org/10.3390/v13091735

Sazonov, I., Grebennikov, D., Meyerhans, A., & Bocharov, G. (2022). Sensitivity of SARS-CoV-2 Life Cycle to IFN Effects and ACE2 Binding Unveiled with a Stochastic Model. *Viruses*, *14*(2), 403. https://doi.org/10.3390/v14020403

Blyuss, K. B., & Kyrychko, Y. N. (2025). Mathematical model of replication–mutation dynamics in coronaviruses. *Mathematical Biosciences*, *388*, 109518. https://doi.org/10.1016/j.mbs.2025.109518

Lin, J., & Amir, A. (2018). Homeostasis of protein and mRNA concentrations in growing cells. *Nature Communications*, *9*(1). https://doi.org/10.1038/s41467-018-06714-z

Yan, Y., & Lin, J. (2025). *Fitness-driven scaling laws between mRNA and protein levels*. https://doi.org/10.1101/2025.03.13.642951

Acknowledgement
This work was developed during the 2026 PEBBLE BioFusion Workshop at Westlake University in Hangzhou, China, from July 24th to August 4th.